

Wigner function evolution of quantum states in the presence of self-Kerr interaction

— [Source link](#) 

Magdalena Stobińska, Gerard J. Milburn, Krzysztof Wódkiewicz

Institutions: University of Erlangen-Nuremberg, University of Queensland, University of New Mexico

Published on: 09 Jul 2008 - Physical Review A (American Physical Society)

Topics: Wigner distribution function, Phase space formulation, Coherent states, Wigner quasiprobability distribution and Quantum tomography

Related papers:

- [Quantum Optics in Phase Space: SCHLEICH:QUANTUM OPTICS O-BK](#)
- [Quantum optics in phase space](#)
- [Sub-Planck structure in phase space and its relevance for quantum decoherence](#)
- [Time-frequency domain analogues of phase space sub-planck structures.](#)
- [Sub-Planck phase-space structures and Heisenberg-limited measurements](#)

Share this paper:    

View more about this paper here: <https://typeset.io/papers/wigner-function-evolution-of-quantum-states-in-the-presence-4ctzorgmfn>

Wigner function evolution of quantum states in the presence of self-Kerr interaction

Magdalena Stobińska*

*Institute für Optik, Information und Photonik, Max-Planck Forschungsgruppe, Universität Erlangen-Nürnberg,
Günter-Scharowsky-Strasse 1, Bau 24, D-91058, Germany*

G. J. Milburn

*Centre for Quantum Computer Technology and School of Physical Sciences, The University of Queensland, St Lucia,
Queensland 4072, Australia*

Krzysztof Wódkiewicz†

*Instytut Fizyki Teoretycznej, Uniwersytet Warszawski, Warszawa 00–681, Poland
and Department of Physics and Astronomy, University of New Mexico, Albuquerque, New Mexico 87131, USA*

(Received 8 November 2007; published 9 July 2008)

A Fokker-Planck equation for the Wigner function evolution in a noisy Kerr medium ($\chi^{(3)}$ nonlinearity) is presented. We numerically solved this equation taking a coherent state as an initial condition. The dissipation effects are discussed. We provide examples of quantum interference, sub-Planck phase space structures, and Gaussian vs non-Gaussian dynamical evolution of the state. The results also apply to the description of a nanomechanical resonator with an intrinsic Duffing nonlinearity.

DOI: [10.1103/PhysRevA.78.013810](https://doi.org/10.1103/PhysRevA.78.013810)

PACS number(s): 42.50.Lc, 42.50.Ct, 42.65.–k

I. INTRODUCTION

Nonlinear interaction of light in a medium provides a very useful framework to study various nonclassical properties of quantum states of radiation. These nonclassical properties are usually associated with quantum interference and entanglement. The phase space Wigner distribution function description of quantum states of light is a powerful tool to investigate such nonclassical effects. With the help of the Wigner function one can simply visualize quantum interference. For example, a signature of quantum interference is exhibited in the Wigner function by the nonpositive values and sub-Planck structures [1]. The nonpositive Wigner function is a witness of a nonclassicality and monitors a decoherence process of a quantum state, e.g., a photon-added coherent state in the photon-loss channel [2], photon-subtracted squeezed state [3], Gaussian quadrature-entangled single photon subtracted light pulse [4], two-photon Fock state [5], odd photon number states superposition [6], and coherent states superpositions [7]. The Wigner function has also been used for computing numerically the quantum-mechanical corrections to the classical dynamics of a nanomechanical resonator (its characteristic pattern, the interference fringes, and negative values, served as a signature for a classical to quantum domain transition) [8]; it has been applied in the model of the dynamics of a nanoscale semiconductor laser [9], to list only a few examples of its applications.

The Kerr medium provides one of the simplest nonlinearity for which there exists a simple analytic Wigner function [10] expression. The highly $\chi^{(3)}$ nonlinear systems generated a lot of interest recently due to their applications e.g., to nondemolition measurements [11], quantum computing ar-

chitectures [12], single particle detectors [13]. The well known example of such a medium is an optical fiber. However, the nonlinearity is small in fibers and is often accompanied by other unwanted effects. Enhanced Kerr nonlinearity was studied in terms of electromagnetically induced transparency [14] and was observed in Bose Einstein condensates [15] and cold atoms [16]. Recent proposals predict obtaining enormous Kerr nonlinearity using the Purcell effect [17], Rydberg atoms [13], and interaction of a cavity mode with atoms [18]. The first and last method is predicted to obtain the nonlinearity of nine orders of magnitude higher than natural self-Kerr interactions with negligible losses. The significant nonlinearity has also been observed for nanomechanical resonators [20].

Most of the investigations of the Wigner function of light have been made for steady state situations. The simplicity of the Kerr medium will allow us to study the full time-dependent Wigner function dynamics with or without a quantum noise.

In this paper we present a Fokker-Planck equation which determines the time evolution of the Wigner function in a noisy $\chi^{(3)}$ medium. We solve this equation numerically assuming a coherent state as an initial condition. We discuss first an ideal and then a dissipative Kerr medium. The results obtained for the ideal case reveal the quantum nature of the state under evolution. The coherent state, known as the most classical among all the pure states, becomes a non-Gaussian squeezed state after some time of interaction with the medium. For some specific times it becomes a finite superposition of other coherent states. An interference pattern with the negative values is clearly visible on the plots of its Wigner function. Due to the small value of the $\chi^{(3)}$ nonlinearity and losses in optical fibers such phenomena have never been observed for light; nor for any other system. However, it turns out that not all quantum effects are washed out due to the decoherence. The Fokker-Planck equation allows for a similar state evolution analysis for any other input state.

*magda.stobinska@fuw.edu.pl

†wodkiew@fuw.edu.pl

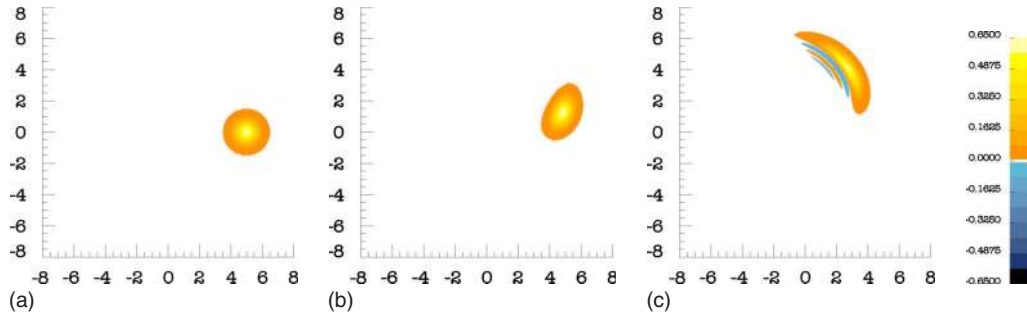


FIG. 1. (Color online) The Wigner function for $\alpha=5$ and $\tau=0$ is a Gaussian function for the coherent state (left). Due to the fact that the evolution in an ideal $\chi^{(3)}$ medium is periodic, we achieve the same shape of the Wigner function for $\tau=2\pi$. The distribution is an ellipse and the state becomes squeezed beginning from $\tau=0.01$ (middle). The negative values of the function start to appear for $\tau=0.04$ (right).

The paper is organized as follows: in Sec. II the Fokker-Planck equation for the Wigner function evolution in a $\chi^{(3)}$ medium is derived from the master equation obtained for a single mode of light density operator. The equation is displayed in polar coordinates. The decoherence effects, losses and thermal noise, are included. The initial and boundary conditions for the Wigner function are set. In Sec. III the numerical results of the Wigner function evolution in a non-dissipative $\chi^{(3)}$ medium are introduced and discussed. These results are obtained using three independent methods: computing the Fokker-Planck equation and the other two equations determining the Wigner function directly, which are obtained from its definition. Correspondence between the Wigner function negative values and zeros of the Q function is noted. In Sec. IV the influence of the decoherence process on quantum effects such as the interference pattern and the negative values of the Wigner function is analyzed. The technical limitations on the use of the Fokker-Planck equation are discussed. The Wigner function sub-Planck structure is shown in Sec. V. In Sec. VI the numerical methods used in Secs. III and IV are compared and discussed. Finally some conclusions are presented.

II. THE FOKKER-PLANCK EQUATION FOR A SELF-KERR INTERACTION

The interaction Hamiltonian for a totally degenerate four-wave mixing process, e.g., in an optical fiber, is of second-order in creation a^\dagger and annihilation a light operators

$$H = \hbar \frac{\kappa}{2} a^\dagger a^\dagger a a, \quad (1)$$

where κ is a nonlinear constant proportional to $\chi^{(3)}$ [21]. Please note that a similar Hamiltonian describes a single nanomechanical resonator with a^\dagger and a being raising and lowering operators related to its position and momentum operators, and κ proportional to the Duffing nonlinearity [19].

In a general case, including damping and thermal noise in the medium, a one-mode density operator evolution, both for light and for a nanomechanical resonator, is determined by the master equation [22]

$$\begin{aligned} \partial_t \rho(\tau) = & -\frac{i}{\hbar} [H, \rho(\tau)] + \frac{\Gamma}{2} ([a\rho(\tau), a^\dagger] + [a, \rho(\tau)a^\dagger]) \\ & + \Gamma M[[a, \rho(\tau)], a^\dagger], \end{aligned} \quad (2)$$

where $\tau = -\kappa t$ is a unitless evolution parameter, t is the interaction time, Γ is a damping constant, $N = 1 / \{\exp(\frac{\hbar\omega}{kT}) - 1\}$ is a mean number of photons in a thermal reservoir.

The solutions of the above equation are well known [21,23–25] but since it is an operator-valued equation, they are inappropriate for computer simulations. A Fokker-Planck type evolution equation for the Wigner function can be easily obtained from Eq. (2) using the standard quantum optics phase space methods [26]. Since every density operator determines its Wigner function uniquely, the knowledge of its evolution is equivalent to the full knowledge of the density operator dynamics.

The dynamics of the Wigner function in a dissipative medium with a self-Kerr interaction is governed by the Fokker-Planck equation, which takes the following form in the polar coordinates $\gamma = r e^{i\varphi}$:

$$\begin{aligned} \partial_\tau W(\tau, r, \varphi) = & \left\{ (r^2 - 1) \partial_\varphi - \frac{1}{16} \left(\frac{1}{r} \partial_r \partial_\varphi + \partial_r^2 \partial_\varphi + \frac{1}{r^2} \partial_\varphi^3 \right) \right. \\ & + \xi + \frac{\xi}{2} \left[r + \frac{1}{2} \left(\frac{1}{2} + N \right) \frac{1}{r} \right] \partial_r \\ & \left. + \frac{\xi}{4} \left(\frac{1}{2} + N \right) \left(\partial_r^2 + \frac{1}{r^2} \partial_\varphi^2 \right) \right\} W(\tau, r, \varphi), \end{aligned} \quad (3)$$

where γ is a point in a phase space, $\xi = \Gamma / \kappa$.

This is a third-order nonlinear differential equation. We compute this equation for the following initial and boundary conditions. The evolution starts with a coherent state $|\alpha\rangle$ described by a Wigner function $W(0, \gamma) = \frac{2}{\pi} e^{-2|\alpha - \gamma|^2}$. The Wigner function tends to zero in the infinity $\lim_{r \rightarrow \infty} W(\tau, r, \varphi) = 0$. Since some of the coefficients in Eq. (3) are singular for $\gamma=0$, we take $W(\tau, 0, 0) = \frac{2}{\pi} e^{-2|\alpha|^2 e^{-\tau\xi}}$, which was derived from the master equation.

III. THE NONLINEAR PART OF EVOLUTION

For $\xi=0$ and $N=0$ the Fokker-Planck equation (3) reduces to its first line and describes the evolution in an ideal Kerr

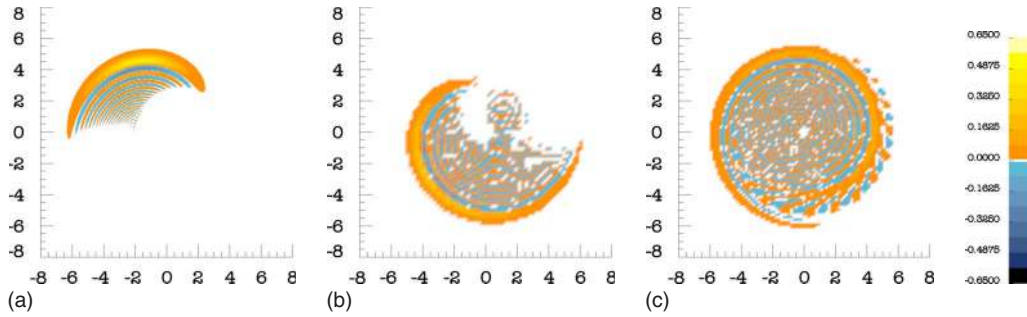


FIG. 2. (Color online) Further steps of Wigner function evolution obtained also for $\alpha=5$ and $\tau=0.08$ (left), $\tau=0.16$ (middle), and $\tau=0.3$ (right). An interference pattern arises in the form of a “tail” of interference fringes.

medium. Figures 1–4 present the plots of the Wigner function for different parameters τ and $\alpha=5$. Due to the fact that the number operator $a^\dagger a$ is a constant of motion, the probability distribution during its evolution will remain situated within a circle of radius $|\alpha|$. Beginning from a circular shape, the Wigner function turns into an ellipse and squeezing appears in an appropriate direction. Then the ellipse changes into a banana shape and a “tail” of the interference fringes appears where the distribution takes the negative values. Squeezing increases and the state becomes non-Gaussian. The “banana part” of the distribution gets thinner in the radial direction and becomes more and more smeared in the azimuthal direction.

The rotation and stretching effects which lead to squeezing are revealed by the first term in the first line of Eq. (3). It shows the dependence of the angular velocity on the distance r from the origin of coordinates. This corresponds to the fact that the nonlinear refractive index $n(\gamma)$ of Kerr medium is intensity dependent $n(\gamma)=n_0+n_2|\gamma|^2$. The intensity fluctuations modulate the nonlinear refractive index and this in turn modulates the phase of traveling light. Photons with stronger amplitude will acquire phase faster than the photons with smaller amplitude.

The other first line terms of this equation consisting of mixed and third order derivatives are responsible for the interference fringes formulation.

If τ is taken as a fraction of the period of the evolution, $\tau=2\pi R$ where $R < 1$ is a rational number, the initial coherent state becomes a superposition of other coherent states, of the same amplitude but different phases; see Fig. 4 [27]. This is also known as a fractional revival [28].

The evolution governed by the self-Kerr interaction Hamiltonian is periodic. It is easy to see this using a unitary evolution operator $U(\tau)=\exp\{-iHt/\hbar\}$ rather than the Fokker-Planck equation approach. Its action on a coherent state $|\alpha\rangle$ expressed in the Fock state basis

$$|\Psi(\alpha, \tau)\rangle = U(\tau)|\alpha\rangle = e^{-|\alpha|^2/2} \sum_{n=0}^{\infty} \frac{\alpha^n}{\sqrt{n!}} e^{i\pi 2n(n-1)} |n\rangle \quad (4)$$

shows that $|\Psi(\alpha, \tau)\rangle = |\Psi(\alpha, \tau+2\pi)\rangle$. In particular, for $\tau=2k\pi$ where k is an integer, Eq. (4) reduces again to the coherent state $|\alpha\rangle$. The same periodicity holds for the Wigner function. This condition has been used as an additional check point in our numerical simulations.

For the wave function given by Eq. (4) one can determine the Wigner function as an analytical function of the evolution parameter τ using the definition [29]

$$W(\tau, \gamma) = \frac{2}{\pi^2} e^{2|\gamma|^2} \int d^2\beta (-\beta|\rho(\alpha, \tau)|\beta\rangle e^{-2(\beta\gamma^* - \beta^*\gamma)}, \quad (5)$$

where $\rho(\alpha, \tau)$ is the density operator of the state $|\Psi(\alpha, \tau)\rangle$. We apply the above equation and express it in two equivalent ways which have been used to obtain the numerical results for the nondissipative Kerr medium

$$W(\tau, \gamma) = \frac{2}{\pi} e^{-2|\gamma|^2} e^{-|\alpha|^2} \sum_{q=0}^{\infty} \frac{(2\alpha^* \gamma e^{i\pi/2})^q}{q!} e^{-i\pi/2 q^2} \times \sum_{k=0}^{\infty} \frac{(2\alpha \gamma^* e^{-i\pi/2})^k}{k!} e^{i\pi/2 k^2} e^{-|\alpha|^2 e^{i\pi(k-q)}}, \quad (6)$$

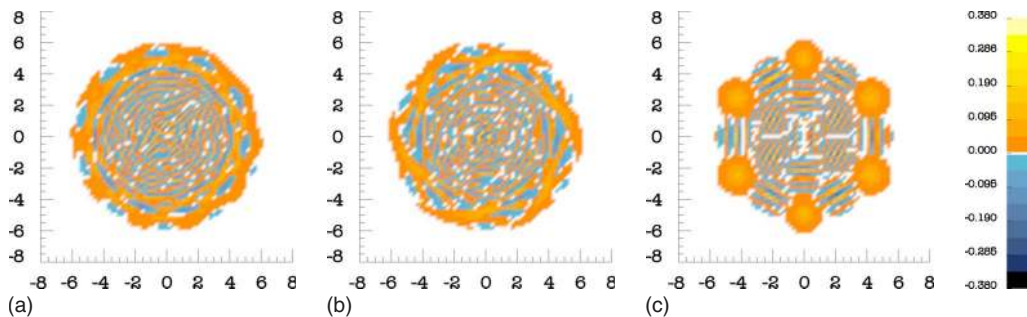


FIG. 3. (Color online) For the evolution parameter values close to $\tau=2\pi R$, where $R < 1$ is a rational number, in some areas a destructive interference starts to dominate—left ($\tau=0.6$) and middle figures ($\tau=1$), thus leading to a Wigner function of a coherent superposition state—right figure ($\tau=\pi/3$). Figures evaluated for $\alpha=5$.

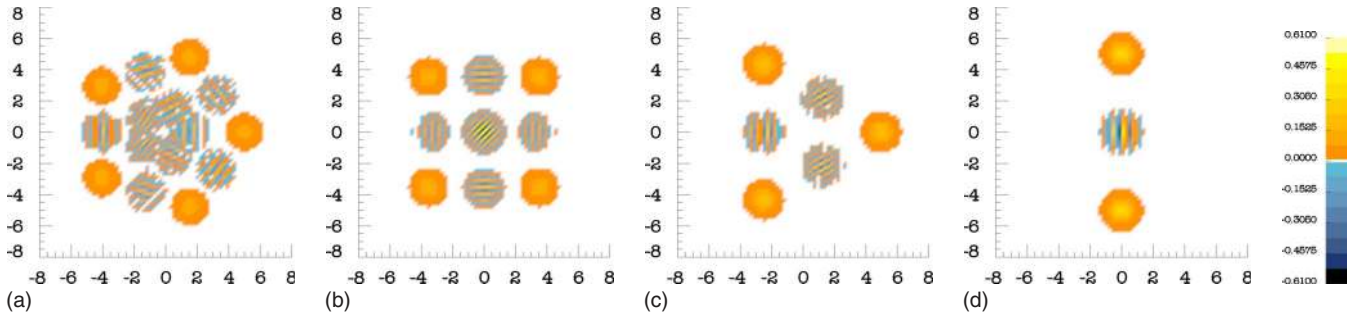


FIG. 4. (Color online) The superposition states obtained for $\alpha=5$ and $\tau=2\pi/5$ (left), $\tau=\pi/2$ (the compass state) (left middle), $\tau=2\pi/3$ (right middle), and $\tau=\pi$ (the Schrödinger cat state) (right).

$$W(\tau, \gamma) = \frac{2}{\pi} e^{2|\gamma|^2} e^{-|\alpha|^2} \sum_{n,m=0}^{\infty} \frac{1}{(-2)^{n+m}} \frac{\alpha^n \alpha^{*m}}{n! m!} e^{i\pi/2[n(n-1)-m(m-1)]} \times (\partial_\gamma)^n (\partial_{\gamma^*})^m e^{-4|\gamma|^2}. \quad (7)$$

Equations (4) and (7) explain how the interference fringes arise from the interference of the Fock number states $|n\rangle$. By virtue of Eq. (7), the Wigner function can be viewed as a sum of the two components: the first one, independent of τ , being a superposition of the Fock states' Wigner functions $W_{|n\rangle\langle n|}(\gamma)$, and the second, being an evolution dependent component $f(\tau, \gamma)$, responsible for the evolution of the fringes,

$$W(\tau, \gamma) = \frac{e^{-|\alpha|^2}}{\pi} \sum_{n=0}^{\infty} \frac{|\alpha|^{2n}}{n!} W_{|n\rangle\langle n|}(\gamma) + f(\tau, \gamma). \quad (8)$$

Although Eqs. (6) and (7) are special solutions of the Fokker-Planck equation, we obtained them separately to proceed with independent computation.

The effects of squeezing and error contour rotation in the phase space can also be observed by studying the easy-to-compute Q function evolution $Q(\tau, \gamma) = 1/\pi \langle \gamma | \rho(\alpha, \tau) | \gamma \rangle$,

$$Q(\tau, \gamma) = \frac{1}{\pi} e^{-|\alpha|^2 - |\gamma|^2} \left| \sum_n \frac{(\alpha \gamma^*)^n}{n!} e^{i\pi/2 n(n-1)} \right|^2. \quad (9)$$

The contour plot of the Q function is plotted in [21]. Solutions of the Fokker-Planck equation for the Q function in a dissipative and noisy Kerr medium have been widely studied

[21,23–25]. Negativities achieved in the Wigner function correspond to zeros of the Q function [30].

All of Figs. 1–4 have been obtained computing Eqs. (3), (6), and (7) independently.

IV. DISSIPATION EFFECTS

In the presence of damping the Wigner function will not remain situated within at the circle of the radius $|\alpha|$ any more. The second line in the Fokker-Planck equation, proportional to the first radial derivative, makes the Wigner function move toward the origin of the coordinates. This effect corresponds to the decreasing number of quanta in the state during the evolution. At the origin the state becomes a vacuum. The third line describes the effects of dispersion.

It is interesting to note an interplay between the nonlinear evolution and damping terms in the Fokker-Planck equation. If damping is negligible, the numerical simulations obtained for small $|\alpha| \approx 1$ and large $|\alpha| \gg 1$ initial amplitudes are very similar. At the beginning of evolution the squeezing effect dominates and then the interference appears. It is not the case if the losses are included in the simulations. If the amplitude is too small the decoherence washes out all the quantum effects and the Gaussian Wigner function located at the coordinates' origin, genuine to a vacuum state, is obtained very quickly.

We proceed the numerical computation for experimentally reasonable values genuine to a nanomechanical resonator. The nonlinear constant $\kappa \approx 2 \times 10^{-4} \text{ s}^{-1}$ and the damping constant $\Gamma \approx 10^3 \text{ s}^{-1}$ ($\xi = 10^5$). The thermal noise coefficient

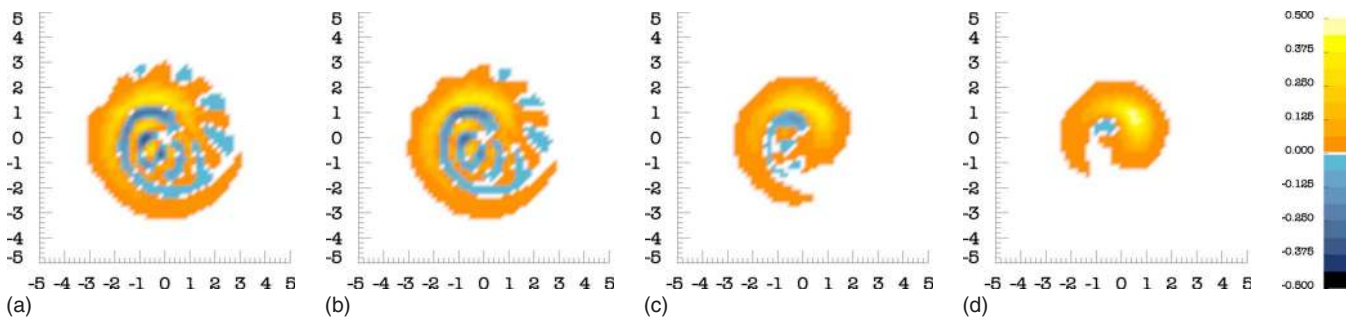


FIG. 5. (Color online) The effect of the decoherence on the Wigner function evaluated for $\alpha=2$, $\tau=0.2\pi$, the thermal noise $N=3.8 \times 10^{-19}$, and the different values of the damping constant: $\xi=0$ (left), $\xi=0.1$ (left middle), $\xi=1$ (right middle), $\xi=2$ (right). Note that the thermal noise gives no input if $\xi=0$.

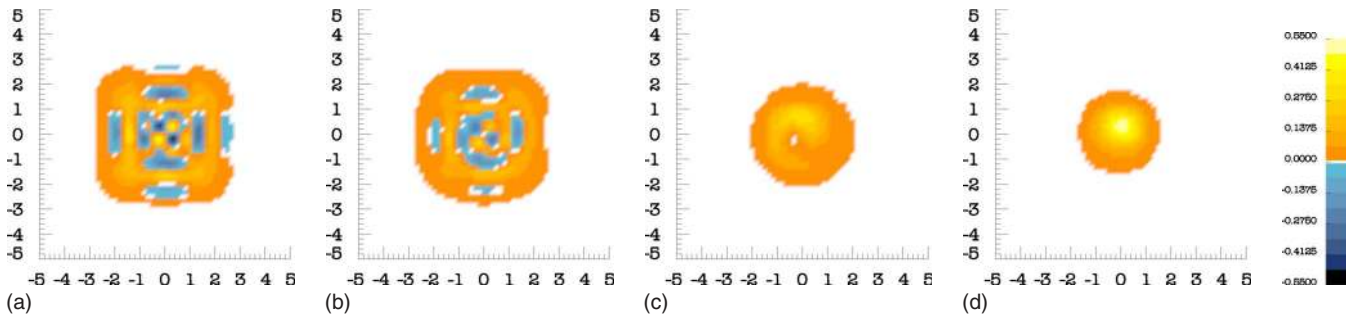


FIG. 6. (Color online) The coherent superposition states are extremely fragile to the decoherence process. The Wigner function of four coherent state superposition ($\tau = \pi/2$) of the amplitude $\alpha=2$ evaluated including the thermal noise $N=3.8 \times 10^{-19}$ and the damping constant equal to $\xi=0$ (left), $\xi=0.1$ (left middle), $\xi=1$ (right middle), $\xi=2$ (right).

in the room temperature is equal to $N \approx 1.9 \times 10^{-14}$.

The nonlinear evolution term r^2 for $\tau \approx 0$ becomes meaningful if $r \approx |\alpha|$. If $|\alpha| \approx 1$ the damping term $\frac{\xi r}{2} \approx 0.5 \times 10^5$ dominates over the nonlinear $r^2 \approx 1$ and interference terms. The coherent state will be almost immediately radially displaced toward the origin of coordinates. For $|\alpha| \approx 10^5$ all the effects are in balance: $r^2 \approx 10^{10}$ and $\frac{\xi r}{2} \approx 0.5 \times 10^{10}$.

Computing the Fokker-Planck equation for such large values of coefficients ($\alpha \approx 10^5$, $\xi \approx 10^5$, $N = 1.9 \times 10^{-14}$) would require a very dense and large grid, thus a lot of computer memory. Therefore, to visualize an influence of these two effects on the Wigner function, we rescaled the parameters.

As we pointed out above, in order to see the nonlinear effects during the Wigner function evolution in presence of dissipation, the input of the nonlinear term has to be of the same order as the dissipation term is. Therefore we keep the ratio between them constant and equal to the ratio evaluated for the nonrescaled case: $\xi \approx \alpha$ and $N = 1.9 \times 10^{-19} \xi$. For $\alpha = 2$ they are equal to $\xi \approx 2$ and $N = 3.8 \times 10^{-19}$. Although such a small value of the thermal coefficient implies a negligible effect on the evolution, we included it in the simulation. Such simulations are accessible using a standard personal computer with 4 GB of memory.

Figures 5–8 present the numerical simulations of the Fokker-Planck equation obtained for $\alpha=2$, $N=3.8 \times 10^{-19}$, and the following values of the damping constant: $\xi=0$, $\xi=0.1$, $\xi=1$, $\xi=2$.

Due to the fact that damping washes out the interference effects, any nonzero damping constant prevents both coherent superposition state formulation and periodicity of the

evolution. As is well known [31] these states are extremely fragile to the decoherence. The areas where the Wigner function takes the negative values disappear; see Fig. 5. For an ideal $\chi^{(3)}$ medium the negativities show up for $0.08 + 2k\pi < \tau < 6.20 + 2k\pi$ where k is an integer. If $\xi=0.1$ the negativities are present for $0.08 < \tau < 5.80$. However, they do not appear in the second round $[(0.08 + 2\pi < \tau < 5.80 + 2\pi)]$. If $\xi=1$ the negative values are present only for $0.08 < \tau < 1.52$ and for $0.08 < \tau < 0.89$ if $\xi=2$.

The Wigner function obtained for the coherent superposition states evolution times $\tau = \frac{\pi}{2}$, $\tau = \pi$, and $\tau = 2\pi$ is depicted in Figs. 6–8. For $\xi=0.1$ the structure of superposition coherent states is still well preserved. However, some additional circular trails are present. These are especially visible for $\tau = \pi$ and $\tau = 2\pi$. For $\xi=2$ and $\tau = \frac{\pi}{2}$ the state is already a vacuum. The vacuum state is achieved for $\tau = \pi$ ($\tau = 10\pi$) if $\xi=1$ ($\xi=0.1$).

V. SUB-PLANCK STRUCTURE IN PHASE SPACE

In the framework of quantum mechanics, it has been recognized that small structures on the sub-Planck scale do show up in quantum linear superpositions [32,33]. Such sub-Planck structures can be shown, if the Wigner function is plotted in a phase space region below the Heisenberg relation. That means in the phase space volume less than 1, since $\Delta X_1 \Delta X_2 \geq 1$ for the amplitude X_1 and phase X_2 quadratures. The quadratures are given by the annihilation $a = \frac{1}{2}(X_1 + iX_2)$ and creation $a^\dagger = \frac{1}{2}(X_1 - iX_2)$ operators and their mean values

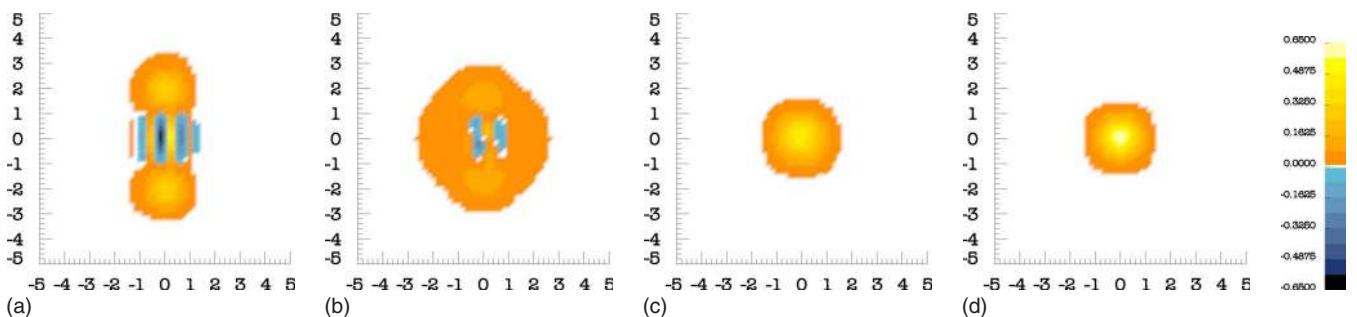


FIG. 7. (Color online) The decoherence looks similarly for the two coherent state superposition Wigner function ($\tau = \pi$), also of amplitude $\alpha=2$, the same thermal noise $N=3.8 \times 10^{-19}$ and the damping constants: $\xi=0$ (left), $\xi=0.1$ (left middle), $\xi=1$ (right middle), $\xi=2$ (right).

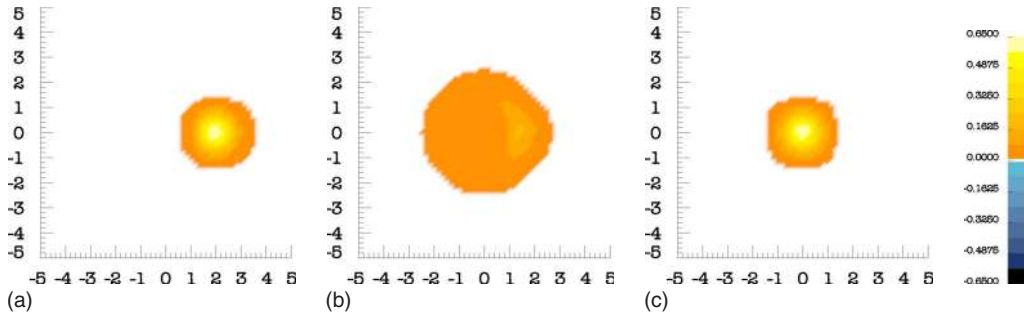


FIG. 8. (Color online) The Wigner function evolution in a noisy $\chi^{(3)}$ medium is not periodic any more. The distribution evaluated for $\alpha=2$, $\tau=2\pi$, the thermal noise $N=3.8 \times 10^{-19}$ and the damping constant equal to $\xi=0$ (left), $\xi=0.1$ (middle), $\xi=1$ (right). The state pursues vacuum.

correspond to phase space coordinates in the following way: $\langle X_1 \rangle = \text{Re } \gamma$, $\langle X_2 \rangle = \text{Im } \gamma$.

Figure 9 compares behavior of the sub-Planck structure of the Wigner function obtained for the compass state ($\tau = \pi/2$) and the Schrödinger cat state ($\tau = \pi$) for $\alpha=2$ in the ideal $\chi^{(3)}$ medium and in presence of damping ($\xi=0.1$). The regions of the opposite sign, in the form of “dots,” are clearly visible. They become flattened and smeared by the damping effects.

The sub-Planck structure is also present for the rational values of evolution parameter, for which the state (4) does not correspond to any coherent superposition state. It is depicted on Fig. 10 for $\tau=0.16$, $\tau=0.3$, $\tau=0.6$, $\tau=1$, and $\alpha=5$. This structure is of different form. The areas of positive and negative values form “ribbons.”

VI. COMPARISON OF THE NUMERICAL METHODS

Figures 1–4, presenting the Wigner function evolution in an ideal $\chi^{(3)}$ medium, have been obtained by three independent numerical simulations: computing Eqs. (3), (6), and (7). The numerical results of the evolution in a noisy medium have been achieved using only the Fokker-Planck equation (3).

All programs used to simulate the Wigner function were written in standard C++ language, due to its high speed and good portability. The structure of the programs used for computation of the Eqs. (6) and (7) was based strictly on these equations: they both consist of two loops which iterate on q

and k (or m and n , respectively) and sum up the evaluated coefficients for a given τ and γ . Common terms were moved out from the loops (especially the inner one) to optimize the evaluation of the sums. The main function was enclosed in input and output logic which calls for different values of γ and writes the results to a file.

Equations (6) and (7) involve summation of the infinite series. However, only a finite number of their terms can be computed. Therefore, assuming a given precision of the simulation, we cut the series off.

The series in Eq. (6) is much more slowly convergent than the series in Eq. (7) because it contains the fast oscillating exponential term $e^{-|\alpha|^2 e^{i\pi(k-q)}}$. Depending on the phase factor in the exponent, this term can take either large or small values, which makes it impossible to compute Eq. (6) using the standard double precision floating point number representation. Therefore for $|\alpha| \leq 5$ both infinite sums, internal and external, are cut off by including at least 500 terms in each of them. Also very high precision (at least 25 significant digits) needs to be applied for the computation. Such a high precision was obtained using the free Class Library for Numbers (CLN) and its long float type.

On the contrary, it is enough to use standard double precision numbers to compute Eq. (7). However, we also applied the CLN here due to the fact that it can deal with the complex numbers while C++ itself cannot. The same precision was used while computing Eq. (7), however, it was enough to take 100 terms in both sums into account to obtain the same results as these which were achieved by computing

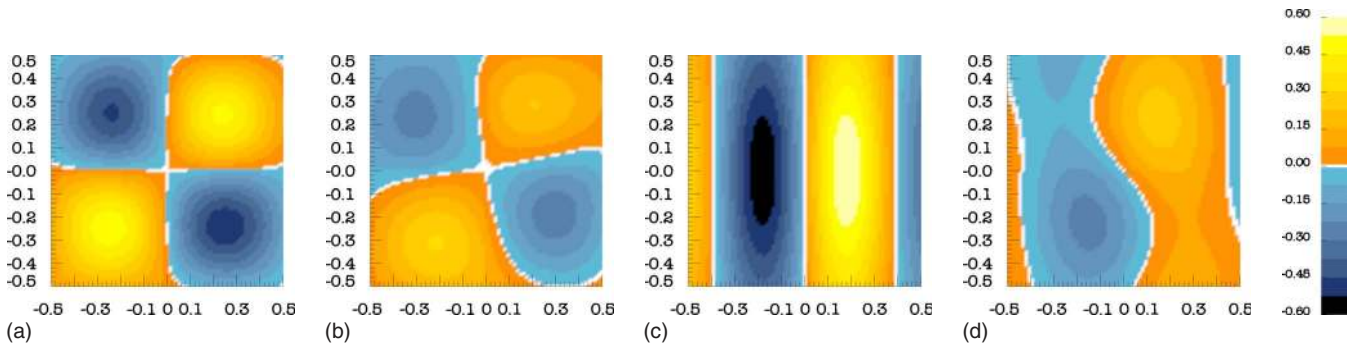


FIG. 9. (Color online) A sub-Planck structure of the Wigner function for $\tau = \pi/2$ and $\xi=0$ (left), $\tau = \pi/2$ and $\xi=0.1$ (left middle), $\tau = \pi$ and $\xi=0$ (right middle), $\tau = \pi$ and $\xi=0.1$ (right).

Eq. (6). This made simulations of Eq. (7) much faster. Additionally, the product of the exponents' derivatives was replaced with the following formula [34]:

$$\begin{aligned} (\partial_\gamma)^n (\partial_{\gamma^*})^m e^{-4|\gamma|^2} &= \sum_{k=0}^n \binom{n}{k} (\partial_\gamma)^k (-4\gamma)^m (\partial_\gamma)^{n-k} e^{-4|\gamma|^2} \\ &= e^{-4|\gamma|^2} \sum_{k=0}^{\min(n,m)} \binom{n}{k} \frac{m!}{(m-k)!} \\ &\quad \times (-4\gamma)^{m-k} (-4\gamma^*)^{n-k}. \end{aligned} \quad (10)$$

Both methods, Eqs. (6) and (7), allow for computation of the Wigner function for an arbitrary evolution parameter τ and point γ in the phase space. Evaluation of the function for a chosen τ does not require simulation of the whole evolution. To visualize the Wigner function we calculated it for each point of a 100×100 square mesh of the size proportional to the value of α ($-5 \cdots 5$ for $\alpha=2$, $-8 \cdots 8$ for $\alpha=5$, $-\frac{1}{2} \cdots \frac{1}{2}$ for sub-Planck structures), to show all interesting aspects of the simulated function.

On the contrary, numerical simulation of the Fokker-Planck equation (3) involves solving a partial differential equation (PDE), which in turn requires setting a grid (discretized phase space) and solving a set of linear equations (one equation for each point of the grid) at each time step.

To solve the PDE, Eq. (3) was rewritten to difference quotient form, where all the partial derivatives were replaced with appropriate difference quotients of fourth order to keep the order of the quotients even and higher than the order of the equation at the same time. Even difference quotients are more convenient, since they are symmetric with respect to the point where the derivative is taken. The quotients were determined using the MATHEMATICA program and its FiniteDifferencePolynomial function. We used polar mesh coordinates with constant radial distance Δr and constant angle $\Delta\varphi$ between points. Below we present the first, second, and third derivatives discretized up to the fourth order:

$$\partial_x \rightarrow \frac{f_{k-2} - 8f_{k-1} + 8f_{k+1} - f_{k+2}}{12h}, \quad (11)$$

$$\partial_x^2 \rightarrow \frac{-f_{k-2} + 16f_{k-1} - 30f_k + 16f_{k+1} - f_{k+2}}{12h^2}, \quad (12)$$

$$\partial_x^3 \rightarrow \frac{-f_{k-2} + 2f_{k-1} - 2f_{k+1} + f_{k+2}}{2h^3}, \quad (13)$$

where $x=r, \varphi$, $h=\Delta r, \Delta\varphi$, and $k=i, j$ for r and φ , respectively, f_k is the Wigner function value. The mixed derivatives were built up combining the above basic formulas.

Since the standard *explicit* computation methods turned out to be unstable due to the large number of time steps, we applied the *implicit* method. At the same time, it also allowed for larger time steps. The main idea of the *implicit* method is to determine the time derivative between steps τ and $\tau+\Delta\tau$ using the spatial derivatives obtained from the next time step $W(\tau+\Delta\tau, \gamma, \gamma^*)$, not from the previous one, $W(\tau, \gamma, \gamma^*)$. This method requires solving a set of linear equations, with Wigner function values in the next time step $W(\tau+\Delta\tau, \gamma, \gamma^*)$ for each point γ of the mesh as unknowns. The stability of this method relies on a well-chosen ratio of the time step and the grid density. For $\alpha=2$ we used time step $\Delta\tau = \frac{\pi}{3600}$ and the grid consisting of 300(radial direction) \times 540(azimuthal direction) points. Thus there were 162×10^3 points and equations in the set.

In order to solve such a large set of equations, we put it in a matrix form. To achieve it we assigned an index i for each point of the polar mesh using the formula $i=N_f r/\Delta r + \varphi/\Delta\varphi$, where N_f is a density of the grid in the azimuthal direction, r and φ are polar coordinates of a point of the mesh, and Δr and $\Delta\varphi$ are radial and angular distances between mesh points. This index was then used as a coordinate to the row and column of the matrix where the coefficients of the equations were placed and to rewrite the Wigner function values of the previous time step from grid to vector form and the result from vector back to mesh form.

The index i (described above) was chosen in such a way that the matrix of equation coefficients is a sparse band matrix. The sample of such matrix computed for small mesh size is depicted in Fig. 11. Black points represent nonzero items (single numbers). It consists of five diagonal five-element bands and an additional two including either two or one elements. In practice, the matrix is much larger and has $162 \times 10^3 \times 162 \times 10^3$ elements, but the characteristic band diagonal structure with five-element bands is preserved.

The set of equations is solved using the band diagonal systems method [35]: the matrix is inverted applying LU decomposition (Crout method) and then solved with Gaussian elimination while keeping the matrices in special compressed form to save computer memory. We used the bandec

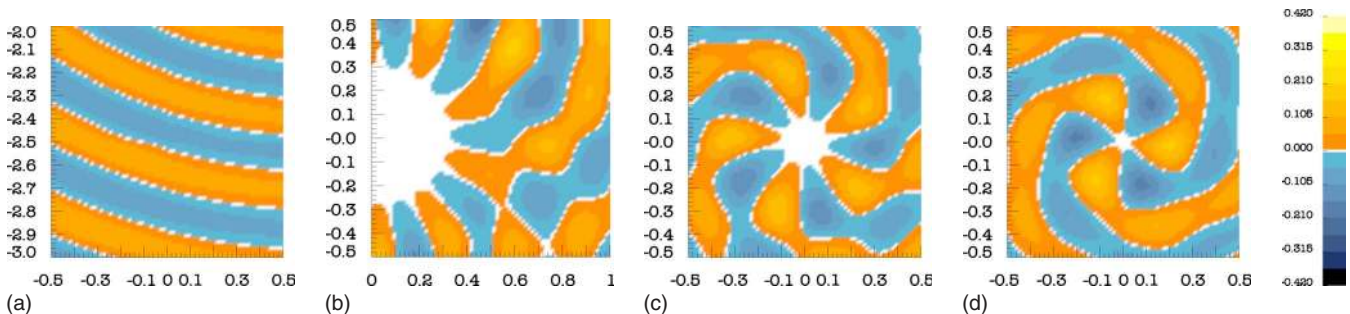


FIG. 10. (Color online) A sub-Planck structure of the Wigner function evaluated for $\tau=0.16$, $\tau=0.3$, $\tau=0.6$, $\tau=1$.

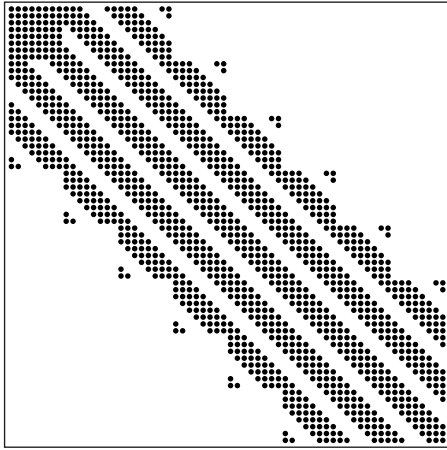


FIG. 11. The sparse band matrix necessary to invert to solve the set of linear equations giving the Wigner function values for all points of the discretized phase space.

and `banmul` routines from [35], translated to C++ and optimized. We also used standard double precision floating point numbers; there was no need for CLN library. The main computing routine was accompanied by input and output logic used to read simulation parameters and write out the results.

The flow of the program consisted of an introductory step—performing a LU decomposition and calculating the Wigner function for $\tau=0$ (initial values for each point of the grid)—and a sequence of steps calculating evolution of the Wigner function for each $\tau=\tau_0+n\Delta\tau$. The solution gives the values of the function for all γ at each evolution step.

During the simulation some sanity checks were taken to make sure that the calculations are done properly, e.g., the integral of the Wigner function over the phase space is equal to 1 in each time step. The value of the integral unequal to 1 was a sign of either too small mesh density or too big time step or too small precision of the calculations. We also compared the results of simulation of Eqs. (3), (6), and (7) for the same input parameters. The numerical results are presented using the OPENDX program.

VII. CONCLUSION

In this paper we presented the Fokker-Planck equation which allowed for numerical computation of the full Wigner function evolution governed by the self-Kerr interaction Hamiltonian. This equation can be used for a state analysis for any input state, mixed or pure. We took a coherent state as an input state for the simulation. For a decoherence-free evolution the results have been obtained by three different numerical algorithms. We discussed the influence of the decoherence process on the nonclassicality of the state under evolution. For an exemplary calculation we took into consideration the experimentally reasonable values of the nonlinearity and damping constant for a nanomechanical resonator. We also presented the sub-Planck structure of the Wigner function which arises during the evolution. This equation can be applied to any system described by the self-Kerr interaction.

ACKNOWLEDGMENTS

This work was partially supported by MEN Grants No. 1 PO3B 137 30 (K.W.) and No. N202 021 32/0700 (M.S.).

-
- [1] L. Praxmeyer, P. Wasylczyk, C. Radzewicz, and K. Wódkiewicz, *Phys. Rev. Lett.* **98**, 063901 (2007).
 - [2] S.-B. Li, X.-B. Zou, and G.-C. Guo, *Phys. Rev. A* **75**, 045801 (2007).
 - [3] A. Biswas and G. S. Agarwal, *Phys. Rev. A* **75**, 032104 (2007).
 - [4] A. Ourjoumtsev, A. Dantan, R. Tualle-Brouiri, and Ph. Grangier, *Phys. Rev. Lett.* **98**, 030502 (2007).
 - [5] A. Ourjoumtsev, R. Tualle-Brouiri, and Ph. Grangier, *Phys. Rev. Lett.* **96**, 213601 (2006).
 - [6] J. S. Neergaard-Nielsen, B. Melholt Nielsen, C. Hettich, K. Molmer, and E. S. Polzik, *Phys. Rev. Lett.* **97**, 083604 (2006).
 - [7] H. Jeong, A. P. Lund, and T. C. Ralph, *Phys. Rev. A* **72**, 013801 (2005).
 - [8] I. Katz, A. Retzker, R. Straub, and R. Lifshitz, *Phys. Rev. Lett.* **99**, 040404 (2007).
 - [9] P. Weetman and M. S. Wartak, *Phys. Rev. B* **76**, 035332 (2007).
 - [10] E. Wigner, *Phys. Rev.* **40**, 749 (1932).
 - [11] N. Imoto, H. A. Haus, and Y. Tamamoto, *Phys. Rev. A* **32**, 2287 (1985).
 - [12] Q. A. Turchette, C. J. Hood, W. Lange, H. Mabuchi, and H. J. Kimble, *Phys. Rev. Lett.* **75**, 4710 (1995).
 - [13] A. K. Mohapatra, M. G. Bason, B. Butscher, K. J. Weatherill, and C. S. Adams, e-print arXiv:0804.3273v1.
 - [14] A. Imamoglu, H. Schmidt, G. Woods, and M. Deutsch, *Phys. Rev. Lett.* **79** 1467 (1997); M. J. Werner and A. Imamoglu, *Phys. Rev. A* **61**, 011801(R) (1999).
 - [15] L. V. Hau, S. E. Harris, Z. Dutton, and C. H. Behroozi, *Nature (London)* **397**, 594 (1999).
 - [16] H. Kang and Y. Zhu, *Phys. Rev. Lett.* **91**, 093601 (2003).
 - [17] P. Bermel, A. Rodriguez, J. D. Joannopoulos, and M. Soljacic, *Phys. Rev. Lett.* **99**, 053601 (2007).
 - [18] F. G. S. L. Brandao, M. J. Hartmann, and M. B. Plenio, *New J. Phys.* **10**, 043010 (2008).
 - [19] M. J. Woolley, G. J. Milburn, and Carlton M. Caves, e-print arXiv:0804.4540v1; E. Babourina-Brooks, A. Doherty, and G. J. Milburn, e-print arXiv:0804.3618v1.
 - [20] I. Kozinsky, H. W. Ch. Postma, O. Kogan, A. Husain, and M. L. Roukes, *Phys. Rev. Lett.* **99**, 207201 (2007).
 - [21] R. Tanaš, in *Theory of Non-Classical States of Light*, edited by V. Dodonov and V. I. Man'ko (Taylor & Francis, London, 2003), p. 267.
 - [22] D. F. Walls and G. J. Milburn, *Quantum Optics* (Springer-Verlag, Berlin, 1995).
 - [23] G. J. Milburn and C. A. Holmes, *Phys. Rev. Lett.* **56**, 2237 (1986).
 - [24] D. J. Daniel and G. J. Milburn, *Phys. Rev. A* **39**, 4628 (1989).

- [25] V. Peinova and A. Luks, *Phys. Rev. A* **41**, 414 (1990).
- [26] C. W. Gardiner, *Quantum Noise* (Springer-Verlag, Berlin, 1991).
- [27] M. Stobińska, G. J. Milburn, and K. Wódkiewicz, *Open Syst. Inf. Dyn.* **14**, 81 (2007).
- [28] I. Sh. Averbukh and N. F. Perelman, *Phys. Lett.* **139**, 449 (1989).
- [29] M. O. Scully and M. S. Zubairy, *Quantum Optics* (Cambridge University Press, Cambridge, England, 1997).
- [30] H. J. Korsch, C. Muller, and H. Wiescher, *J. Phys. A* **30**, L677 (1997).
- [31] I. L. Chuang, R. Laflamme, P. W. Shor, and W. H. Zurek, *Science* **270**, 1633 (1995).
- [32] W. H. Zurek, *Nature (London)* **412**, 712 (2001).
- [33] V. N. Shatokhin and S. Ya. Kilin, *Phys. Rev. A* **63**, 023803 (2001).
- [34] I. N. Bronstein and K. A. Semendiajew, *Taschenbuch der Mathematik* (B. G. Teubner Verlagsgesellschaft, Leipzig, 1959).
- [35] W. H. Press, B. P. Flannery, S. A. Teukolsky, and W. T. Vetterling, *Numerical Recipes* (Cambridge University Press, Cambridge, England, 1988).